Contents lists available at ScienceDirect

Journal of Membrane Science

journal homepage: www.elsevier.com/locate/memsci

Energy duty in direct contact membrane distillation of hypersaline brines operating at the water-energy nexus

Enrica Fontananova [**], Valentina Grosso, Elvira Pantuso, Laura Donato, Gianluca Di Profio [*]

Consiglio Nazionale delle Ricerche (CNR), Istituto per la Tecnologia delle Membrane (ITM), via P. Bucci Cubo 17/C, 8036, Rende, CS, Italy

ABSTRACT

In the context of global climate crisis and growing world population there is the urgent need for viable technical solutions to harvest energy from alternative, renewable and continuous sources and to recover pure water at affordable costs. Herein, we capitalize on the study of direct contact membrane distillation technology treating hypersaline solutions simulating reverse electrodialysis outgoing mixed streams, in the logic of valorising the otherwise environmentally threating brine, in an integrated system operating at the water-energy nexus.

Experimental results in terms of transmembrane water flux and dissolved salts rejection, indicate that DCMD is a feasible option to treat feed solutions with concentrations as high as 228 g L^{-1} total dissolved solids, while recovering pure water from brines which are practically impossible to be dewatered through reverse osmosis. Specific thermal energy consumptions and gain to output ratios, calculated under different feed compositions and flow rates for polypropylene and polyvinilidenefluoride membranes, indicated the possibility to tailor the thermal energy requirements of the MD stage by controlling the ratio between the streams at different salinity that are partially mixed in the RED unit and to potentially adapt it to the available amount of heat.

1. Introduction

Global climate change and growing world population urgently request for the decarbonisation of energy supply, by reducing fossil fuel exploitation, and for the farsighted-management of natural resources, particularly water [1–3]. In addition to the increasing demand for agriculture and direct human consumption, water is extensively used in many industries, thus generating large amounts of waste streams. These wastewaters normally contain high dissolved salts concentrations together with several chemical pollutants arising from the process where the water was originally used [4]. If not properly treated before their release in the environment, hypersaline effluents (that is saline solutions of concentration greater than 70,000 ppm [5]) might alter the physicochemical properties of the receiving sites and can cause significant damage to aquatic ecosystems and to public health [6–8]. However, despite the growing concern related to the management of hypersaline

streams, the currently available treatment methods are substantially inadequate, potentially deleterious to the environment and costly [5,9].

Otherwise, hypersaline effluents can be considered as an alternative energy source to fossil fuel when used for electrical power generation from salinity-gradients [10]. In addition to mitigate the threat to ecology caused by their release in the environment [11,12], harvesting salinity gradient power (SGP) from hypersaline streams has the advantage to be renewable and not intermittent [13]. In this respect, reverse electrodialysis (RED) is a membrane technology for the conversion of the free energy of mixing of two solutions at different dissolved salt concentration into electrical power [14]. In the RED system, the osmotic pressure gradient generated by the different concentrations between two streams is directly converted into energy by driving ions across cation-exchange membranes (CEM) and anion-exchange membranes (AEM), stacked together in an alternate order [15]. The maximum amount of electrical energy that can be generated depends on the operating temperature, the

selectivity of the membranes, the internal resistance of the stack, the chemical composition of the dissolved salts and the concentration of the two solutions [16,17].

In this context, Fig. 1 schematizes a case study where a high-salinity stream (HSS) and a low-salinity stream (LSS) are utilized in a RED process to generate electrical power, with the mixed solution downstream to the RED unit that is re-concentrated by solar-driven membrane distillation (MD) [18]. Dewatering the outgoing RED solution by MD will reduce the liquid volume, thus facilitating the subsequent reuse of the concentrated solution as HSS at the RED stage, while the desalinated water will contribute in alleviating water scarcity and enhance water security [19,20].

In recent years, membrane distillation has emerged as a promising technology towards zero liquid discharge (ZLD) and resource recovery, thanks to its ability to effectively treat high concentration solutions [21]. In MD, water vapour and volatiles spontaneously transfer from the feed side to the distillate side, driven by the vapour pressure difference across the hydrophobic and porous membrane, which acts as physical barrier between the two compartments. Pure water (100% theoretical rejection to non-volatile components) is continuously collected at the distillate side, while the feed is simultaneously concentrated and can potentially reach saturation. MD process is currently developed into four main configurations: direct contact (DCMD), air gap (AGMD), vacuum (VMD) and sweep gas (SGMD) membrane distillation [22]. Among them, DCMD is a thermally-driven technology that has been frequently investigated for the treatment of hypersaline solutions whose osmotic pressure lies beyond reverse osmosis (RO) ability. Indeed, while RO is suitable to recover pure water from salty solutions up to ~90,000 ppm TDS, due to the high hydraulic pressure needed to overcome the osmotic pressure that might have irreversible impacts on membrane permeability and selectivity [23], feed concentration has relatively little effect on mass flux for DCMD [24–27]. For instance, DCMD was effectively used for water and chemicals recovery from RO and RED concentrates from petrochemical effluents [28]. It was shown that water recovery up to 70–80% and solute rejection exceeding 99.5% could be achieved to produce water that was suitable for boiler feed make-up. DCMD was operated on RO retentate at 40–50 °C, resulting in a volume reduction factor of 83.6% and transmembrane flux in the range of 1.2–2.4 kg m^{-2} h^{-1}. The MD brine (4.0–5.4 M) was then fed to a RED stage as HSS, with seawater (0.5 M) as LSS [29]. Under this approach, up to 23% reduction in electrical energy consumption and 16.6% decrease in specific energy consumption were achieved when including the RED unit compared to the benchmark flowsheet with only RO [30].

Despite its technical feasibility to concentrate hypersaline streams, the energy input requested for a typical DCMD stage has still a critical impact, while minimizing thermal energy usage is essential for enabling this technology as efficient and sustainable alternative to non-thermal desalination methods [31]. However, only little study has been performed until now on the quantification of the thermal energy input

needed to drive a DCMD stage for the concentration of hypersaline streams.

Herein, we capitalize on the study of a DCMD system used for pure water recovery and the regeneration of simulated RED outgoing mixed solutions whose compositions lay within the range of the different scenarios shown in Fig. 1. Namely, we considered the several possible combinations in the RED stage between the HSS, consisting in synthetic mine tailings wastewater at the concentration 228 g L^{-1} TDS (indicated as "brine"), and the LSS, being simulated well water at 1.21 g L^{-1} TDS (named as "well"), and used as feed to the MD unit. We compared the transmembrane flux, solute rejection, specific thermal energy consumption (*STEC*) and gain to output ratio (*GOR*) at variable flow rates with membranes made of polypropylene (PP) or polyvinilidene fluoride (PVDF) materials. Results highlighted the possibility to tailor the thermal energy requirements of the MD process by controlling the ratio between the two streams that are partially mixed in the RED stage, together with the feed velocity. On the whole, the direct relation between the energetic duties resulting from the several operative conditions clearly show the potentiality to adapt the thermal energy penalty of the DCMD stage to the available amount of heat (e.g. low-grade heat or solar energy), thus making the membrane distillation process energetically affordable for dewatering hypersaline streams in the logic of an integrated RED-MD system operating at the water-energy nexus.

2. Experimental

2.1. Materials

Sodium chloride (NaCl, cod. 27810.295, from VWR Chemicals), sodium hydrogen carbonate (NaHCO$_3$, cod. 1.06329.1000, from Merck), sodium sulfate (Na$_2$SO$_4$, cod 13464, from Honeywell – Fluka), calcium chloride bihydrate (CaCl$_2$·2H$_2$O, cod. C/1500/53, from Fisher Scientific), magnesium chloride hexahydrate (MgCl$_2$·6H$_2$O, cod. 1.0583.1000, From Merck), potassium chloride (KCl, cod. 26764.298, from VWR Chemicals), magnesium sulfate heptahydrate (MgSO$_4$·7H$_2$O, cod. 13142, from Honeywell – Fluka), and calcium nitrate tetrahydrate (Ca (NO$_3$)$_2$·4H$_2$O, cod. C/1882/53, from Fisher Scientific) were used as received to prepare synthetic "brine" and "well" solutions whose compositions are reported in Table 1. Milli-Q water was used to prepare solutions and as condensing fluid on the distillate side in the DCMD plant. Commercial polypropylene and polyvinyldene fluoride membranes were purchased from Membrana GmbH and Millipore, respectively. Physical chemical properties of the membranes are reported in Table 2.

2.2. Contact angle measurements

Static contact angles to pure water and feed solutions were measured with a goniometer (Nordtest, Italy) at ambient temperature. A drop (5
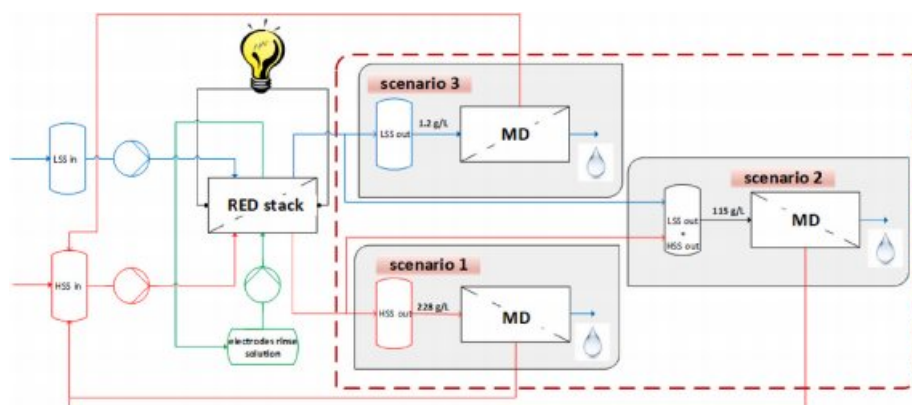
Fig. 1. Scheme of an integrated membrane system where mine tailing brine and well water are used as high-salinity (HSS) and low-salinity (LSS) streams, respectively, for power generation by a RED unit, while a solar-driven MD stage is used to recover fresh water from the mixed outgoing solution and re-concentrate it to recycle in the RED, in view of three possible scenarios of solution composition. (For interpretation of the references to colour in this figure legend, the reader is referred to the Web version of this article.)

Table 1

Average composition of the synthetic solutions simulating brine from mine tailing and well water [32].

Ionic species	Brine [mg L^{-1}]	Well [mg L^{-1}]
Na$^+$	57922.1	73.4
Mg^{2+}	9583.2	106.4
Ca^{2+}	970.9	141.6
K$^+$	20536.1	24.3
Cl$^-$	135696.7	191.7
SO$_4^{2-}$	3534.3	272.8
HCO$_3^-$	126.5	398.6
pH	7.4	7.2
TDS [ppm]	~228370	~1209

μL) of liquid was put onto the membrane surface by a micro-syringe and measurements were carried out by setting the tangents on both visible edges of the droplet, on five different positions for each sample. The average value is reported in Table 2.

2.3. Pore size and porosity

The membrane total porosity was measured by the gravimetric method at 25 °C, determining the weight of filling liquid (Fluorinert FC-40, cod. F9755, from Sigma-Aldrich) contained in the porous matrix. The porosity ε [−] is calculated by the following equation:

$$\varepsilon = \frac{\frac{(w_2-w_1)}{\rho_l}}{\frac{(w_2-w_1)}{\rho_l} + \frac{w_1}{\rho_p}} \qquad (1)$$

where w_1 and w_2 [g] are the weight of the dry and the wet samples, respectively, ρ_l is the density of the Fluorinert (1.85 g cm^{-3}) and ρ_p is the polymer density (0.92 g cm^{-3} for PP and 1.78 g cm^{-3} for PVDF).

2.4. Direct contact membrane distillation tests

Fig. 2A shows the scheme of the experimental DCMD set up used in this work, consisting in: a stainless steel feed reservoir (maximum volume 5 L); a Teflon distilled reservoir (maximum volume 3 L), placed on a balance (model 15000 LCD, Gibertini, Italy); the MD module, in nylon,

for membrane housing; peristaltic pumps (model 323, Watson-Marlow, UK) for solutions circulation; pulsation dampers (from Cole-Parmer, USA); heat exchangers connected to refrigerated & heating circulators (model F32, Julabo, Germany), to generate the thermal gradient; a logic control unit (DeltaE, Italy) connected to a PC.

The inlet and outlet of the membrane module were equipped with electronic platinum resistance thermometers (PT100) and flow rate and pressure meters (from RS Components, Italy). Active membrane area inside the module was 4.8x10^{-3} m^2. Module and all lines of the plant were thermally insulated to minimize the heat loss toward the environment. The starting volume of feed and distillate water were 2 L. The temperature of the feed and the distillate water were set at 60 and 15 °C, respectively. The temperatures of the feed and distillate streams were read at the module inlets and outlets by PT100 probes. For each test, feed and distillate water were circulated counter-currently at the same flow rates of 300-450-600-750-900 mL min^{-1}, corresponding to the axial velocities of 0.024-0.036-0.048-0.061-0.073 m s^{-1}, respectively. Velocities are calculated taking in consideration the cross section flow path dimension and geometry of the membrane module (Fig. 2C). Tests were performed with feed solutions of different composition (see Table 1) to simulate: (i) mine tailing wastewater (brine), (ii) well water (well) and (iii) mixed brine and well at 1:1 vol ratio (well-brine 1:1). Each MD test lasted for 5 h after reaching steady state conditions (normally achieved after 1 h from process start-ups).

The water transmembrane flux J_v [kg m^{-2} h^{-1}] was calculated by registering the increase in distillate weight as a function of time and taken as the average value under steady conditions (normally after the first hour of operation and for the following 5 h), calculated as:

$$J_v = \frac{M_d}{\Delta t \bullet A_m} \qquad (2)$$

where M_d [kg] is the increased mass of distillate, Δt [h] is the distillation time and A_m [m^2] is the active membrane area. The water recovery ratio Rec [%] was calculated by:

$$Rec = \left(\frac{Q_d}{Q_f}\right) \bullet 100 \qquad (3)$$

with Q_d and Q_f [kg h^{-1}] being the distillate and the feed mass flow rate,

Table 2

Properties of PVDF and PP membranes used in this work (Contact angle to: water θ_w; well θ_{we}; well + brine 1:1 volume ratio θ_{w+b}; brine θ_b).

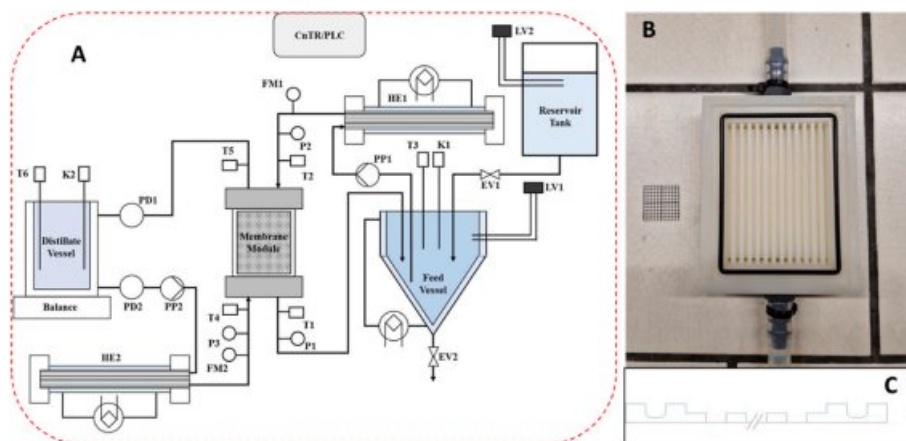| Material	Pore size [μm]	Porosity [-]	Contact angle [°]				Thickness [μm]	Thermal conductivity [33] [W m^{-1} K^{-1}]
			θ_w	θ_{we}	θ_{w+b}	θ_b		
PP	0.2	0.85	135 ± 4	137 ± 2	140 ± 4	140 ± 3	174	0.11–0.16
PVDF	0.2	0.63	139 ± 2	132 ± 2	139 ± 4	140 ± 3	136	0.17–0.19

Fig. 2. (A) Direct contact membrane distillation plant composed by: T1-T6 temperature probes; P1–P3 pressure probes; FM1-FM2 flow-meters; PP1-PP2 peristaltic pumps; EV1-EV2 electro-valves; LV1-LV2 liquid-level probes; HE1-HE2 heat exchangers; PD1-PD2 pulsation dampers; K1–K2 conductivity meters; membrane holder cell; CnTR/PLC logic controller. (B) Membrane module with reference unit (2 × 2 cm^2 graduated square). (C) Cross section of the membrane module perpendicular to the liquid flow path.

respectively. The solute rejection R [%] was determined as:

$$R = \left(1 - \frac{C_d}{C_f}\right) \bullet 100 \qquad (4)$$

where C_d and C_f [g L^{-1}] are the distillate and the feed salt concentrations, respectively, estimated by measuring the electrical conductivity of the solutions (by a Jenway conductivity meter, Bibby Scientific, UK), after mass balance.

The thermal efficiency of the MD system in the different conditions and for the two membrane types, was estimated through calculation of the specific thermal energy consumption $STEC$ [kWh m^{-3}] and the gain to output ratio GOR [−]. The GOR was calculated by:

$$GOR = \frac{J_v \bullet A_m \bullet \Delta H_v}{C_{p,f} \bullet Q_f \bullet \Delta T_f} \qquad (5)$$

where ΔH_v [J kg^{-1}] is the enthalpy of water vaporization from the feed, $C_{p,f}$ [J kg^{-1} K^{-1}] is the specific heat capacity of the stream, ΔT_f [K] is the difference in temperature of the feed stream at the module inlet $T_{f,in}$ and outlet $T_{f,out}$.

The specific thermal energy consumption was calculated by:

$$STEC = \frac{Q_{in}}{Q_d} \qquad (6)$$

where Q_{in} [kW] is the amount of heat supplied through the hot stream, calculated as:

$$Q_{in} = Q_f \bullet C_{p,f} \bullet \Delta T_f \qquad (7)$$

3. Results and discussion

In the context of the integrated RED-MD system of Fig. 1, we studied the performance of the DCMD stage to recover pure water and to concentrate the RED outgoing mixed solution in terms of distillate water quality and thermal energy requirements under various feed solutions velocities v_f and dissolved salt concentrations. Specifically, the three hypothesised scenarios investigated in this work consisted in the use of

synthetic solutions simulating: (i) the brine from mine tailing as HSS, (ii) the well water as LSS, and (iii) the brine and well mixed solution at 1:1 vol ratio, as feed to the MD unit of Fig. 2, with PP and PVDF membranes (physical-chemical properties in Table 2).

Fig. 3A shows the increase in the transmembrane fluxes J_v when the feed solution velocity increases from 2.4×10^{-2} to 7.3×10^{-2} m s^{-1} for all feed solution compositions and for both membrane types, thanks to the higher convective heat and mass transfer generated at larger Reynolds numbers (Eq. S(12)). With simultaneous heat and mass transfer taking place across the membrane, the thermal boundary layer located just adjacent to the membrane surface (Fig. S1) creates a heat resistance and makes the temperature at the liquid–membrane interface lower than that at the bulk of the feed, reducing the effective driving force as a result [34]. This temperature polarization (TP) effect, which is quantified by the temperature polarization coefficient TPC (Eq. S(13)), is considered as one of the most important challenge for MD operations, which has also a higher impact on the reduction of flux in comparison to concentration polarization (CP) effect. It has been reported that up to 80% drop in the driving force can be attributed to TP [35]. In the present case, enhanced mixing conditions generated by the larger feed velocities for high flow rates Q_f allow to increase the convective heat transfer, reducing temperature polarization, while higher mass transfer coefficient and reduced thickness of the boundary layer contribute to the larger driving force between the feed and the distillate sides. This is confirmed in Fig. 3B, showing the increasing trend of TPC with increasing v_f, thanks to the decreased thickness of the heat transfer resistance layer. As a result, the overall membrane mass transfer coefficient B_m increases with the increase of the feed velocity (Fig. 3C).

The asymptotic trend of the curves shown in Fig. 3A and B indicates that the heat and mass transfer in the boundary layer becomes no longer the controlling step at the higher feed velocities, and transmembrane flux is less sensitive to the further increases in v_f, in agreement with other literature data [36–38].

For the same experimental conditions, transmembrane fluxes for PP membranes were always larger than for PVDF samples. As possible reason could be the higher porosity of PP membranes, despite their higher thickness and similar pore size (Table 2).
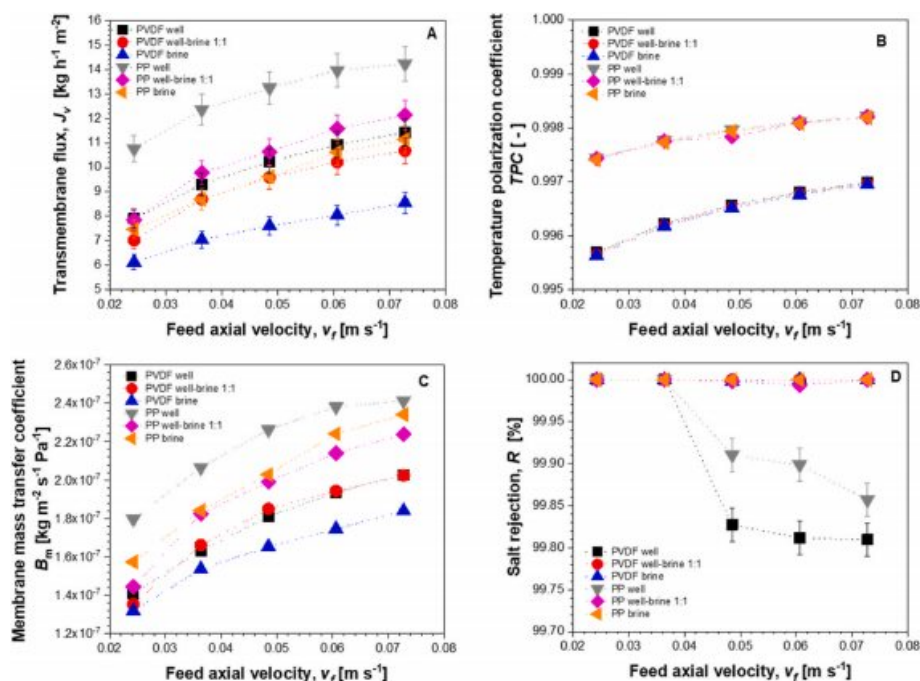

Fig. 3. (A) Transmembrane fluxes J_v, (B) temperature polarization coefficient TPC, (C) overall membrane mass transfer coefficient B_m and (D) salts rejections R, as function of the feed axial velocity v_f for PP and PVDF membranes at different feed solutions concentrations (well: 1.21 g L^{-1}; well-brine 1:1: 115 g L^{-1}; brine: 228 g L^{-1}) (dotted lines are guides for the eyes).

Salts rejections, calculated as the average values over 5 h of continuous operation, were observed close to 100% with the exception of a slight reduction with well solutions at axial velocity exceeding 3.6×10^{-2} m s^{-1} for both membranes types (Fig. 3D). This can be due to the limited amount of salt passing through the membrane because of some wetting effects. This wetting, though minimal, is more evident in the case of dilute well solutions, whose salt concentration is comparable to that of the water used on the distillate side as condensing fluid.

As the feed concentration C_f increases from 1.21 g L^{-1} (well) to 228 g L^{-1} (brine), the progressive reduction in J_v is observed for both PP and PVDF membranes (Fig. 4A and B). Although it is generally known the minimal effect of feed concentration on the performance of the MD process [39], that makes a significant advantage of this technology compared to RO for the concentration of high-salinity solutions, in the present study a visible reduction in transmembrane flux is observed for increasing feed salinity. Fig. 3B clearly demonstrate that feed concentration has a negligible effect on the thermal polarization in the range of investigated conditions. With the increase in C_f, the thermal conductivity of the solution decreases only by 1.6% (from 649.2 to 638.8 mW m^{-1} K^{-1}) [40,41], which makes minor effect on TP. Furthermore, with the increase in the feed concentration, both solution density and viscosity increase [40], affecting the Reynolds number in the opposite way (Eq. S(12)). At 59 °C, that is the average inlet temperature in our experiments, the density increases of about 17% while the dynamic viscosity increases by more than 80%, so that Re (for $v_f = 7.3 \times 10^{-2}$ m s^{-1}) decreases from 460 to 298, affecting heat and mass transfer coefficient (Eqs. S9 and S10). Also, the water vapour pressure of the feed decreases with salinity (Eq. S(4)): it is estimated a water partial pressure drop of 15.8% for 228,000 ppm NaCl solution relative to 1,210 ppm [42]. The overall result of these contributes is the increase of the boundary layer that impacts on the heat and mass transfer coefficients at different extent, thus allowing the driving force for water evaporation, and the transmembrane flux, to decline. This can be seen in Fig. 4C and D that show the variation of B_m with increasing feed concentration for both membranes, in agreement with other works [43].

In Table 3 we report the percent difference (% reduction) of transmembrane flux (ΔJ_v), calculated from data of Fig. 3A, between the

condition of lowest (1.21 g L^{-1}) and highest (228 g L^{-1}) feed concentrations at the same solution velocity, for the two membrane types. In the case of PP membranes, increasing v_f is found to have a beneficial effect on the decline of J_v, contributing to mitigate the influence of the feed salinity on the mass transport. This suggests that for these membranes the transfer of mass and heat from the bulk solution towards the boundary layer is the limiting step in the overall transport mechanism within the range of investigated conditions. For PVDF membranes, the impact of the feed velocity on the decline of J_v for increasing solution concentration is first detrimental, since ΔJ_v becomes more negative, while for $v_f > 6.1 \times 10^{-2}$ m s^{-1} a positive contribute is observed. Therefore, for PVDF membranes, the rate of heat and mass transfer within the boundary layer in the low region of feed velocities is no longer the governing factor in the water evaporation process. On the contrary, the reduced contact time between the fluid and the membrane surface for increasing feed flow rate, combined with the less efficient conversion of the input thermal energy in latent heat of evaporation (see below) for the PVDF material, provides a negative influence on the rate of mass transfer across the membrane. This effect is overcome only at the upper range of v_f, where the improved fluid-dynamics conditions begin to generate a positive influence.

Energy calculations allow to assess the performances of the MD process in the re-concentration of simulated RED outgoing solutions for the several operating scenarios of Fig. 1. Different factors have influence

Table 3

Percent reduction of transmembrane flux ΔJ_v between conditions of feed concentration 1.21 and 228 g L^{-1} at different feed solution velocity, for PP and PVDF membranes.

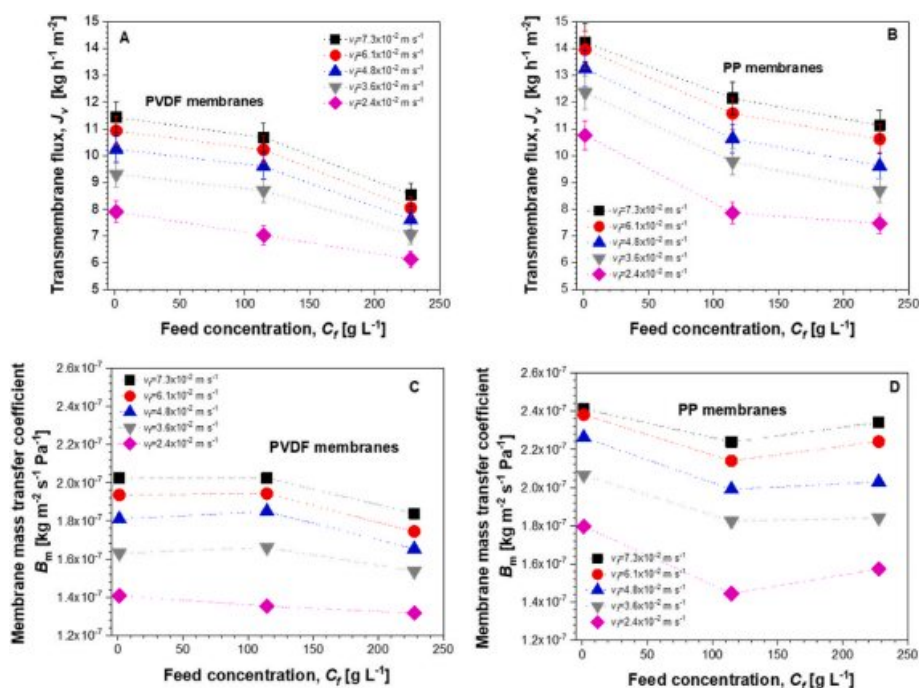| v_f [m s^{-1}]	ΔJ_v [%]	
	PP	PVDF
2.4×10^{-2}	−30.6	−22.4
3.6×10^{-2}	−29.6	−24.2
4.8×10^{-2}	−27.4	−25.7
6.1×10^{-2}	−23.9	−26.3
7.3×10^{-2}	−21.7	−25.2

Fig. 4. Transmembrane fluxes J_v (A and B) and overall membrane mass transfer coefficient B_m (C and D) at several feed concentration C_f for PVDF (A and C) and PP (B and D) membranes (dotted lines are guides for the eyes).

on the energy consumption in MD processes, including membrane materials and feed stream quality [44]. Primarily, in a thermally activated process like DCMD, a large amount of energy is consumed for the evaporation of water [45,46]. Depending on the salinity of the feed, the enthalpy of water vaporization, or latent heat (ΔH_v), at ambient conditions is around to 2400 kJ kg^{-1} [47]. In the present case, assuming an average feed temperature of 59 °C, ΔH_v varied slightly around 2360 kJ kg^{-1} [48].

Fig. 5A and B shows the heat input rate Q_{in} calculated by Eq. (7) for the different conditions investigated in this work. Q_{in} is directly proportional to the feed solution velocity v_f (through the flow rate Q_f, being $v_f = Q_f/A$, with A the cross section area of the fluid path within the membrane module), the specific heat capacity of the feed $C_{p,f}$ and the difference in temperature ΔT_f between the inlet and the outlet stream on the hot side of the membrane module. Based on this definition, Q_{in} denotes the amount of heat released by the mass of flowing fluid at the feed side that is transferred to the distillate side within the pores as latent heat for water vaporization, plus the heat conducted through the solid portion of the membrane and through the stagnant air within the pores (plus the heat losses with the environment). The different weights of all these contributes to Q_{in} for the two membrane types explain the shape of the curves observed in Fig. 5A and B, emphasizing the different behaviours between the two membrane materials and structures.

For both membranes it is seen the largest energy input is obtained when the concentration of the feed is the lowest (Fig. 5A and B). The reason behind this is the larger amount of heat consumed to evaporate water at higher flow rates (higher J_v for decreasing feed concentration in Fig. 4A and B) that affects ΔT_f. Fig. 5C shows the decrease of ΔT_f with increased feed concentration, that is more visible for PVDF than PP membranes, in particular when going from well-brine to brine solutions. This is reflected in Fig. 5B, that shows for PVDF membranes the progressive reduction in the energy input rate with increasing solution salinity for all velocities and the larger step decrease in Q_{in} passing from 115 to 228 g L^{-1} of feed concentration. Furthermore, both the thermal conductivity and the specific heat capacity of saline solutions are known

to decrease with higher dissolved salt concentration [41,49]. Increasing NaCl concentration from 1.2 to 228 g L^{-1} at 59 °C implies a reduction in thermal conductivity of about 1.6% (from 649.2 to 638.8 mW m^{-1} K^{-1}). This contributes somewhat to the increase in TP because of the larger resistance to heat transfer from the bulk towards the evaporation interface at the feed side, which decreases the rate of water evaporation and the amount of consumed heat. For the same increase in salt concentration (from 1.2 to 228 g L^{-1}), $C_{p,f}$ decreases by more than 21% (from 4.18 to 3.29 kJ kg^{-1} K^{-1}), thus contributing directly to the decrease of Q_{in} (Eq. (7)). The heavy influence of the thermal boundary layer, together with the concentration boundary layer, that are connected to salt concentration for PVDF membranes, has a role in their lower process performances, particularly at lower solution velocities. Indeed, for PVDF membranes, a transitional regime is observed in Fig. 5A, where the contribute of the increased solution velocity through the flow rate (direct relation between Q_{in} and Q_f in Eq. (7)) first prevails and drives Q_{in} to rise up to a maximum achieved for $v_f = 4.8 \times 10^{-2}$ m s^{-1}. As solution velocity increases further, Q_{in} start to decrease under the larger effect of the reduction in ΔT_f due to the reduced retention time of the fluid in contact with the membrane surface as Q_f increases. Since the ΔT_f decreases almost linearly with the feed velocity (Fig. 5C), the non-monotonic shape of the Q_{in} vs. v_f curves is observed. Physically, in the low v_f regime ($<4.8 \times 10^{-2}$ m s^{-1}), owing to the lesser impact of the fluid velocity on the thickness of the boundary layer compared to the heat transfer rate across the PVDF membrane, Q_{in} increases with v_f. As the feed velocity overcomes this limiting value, the improved mixing conditions facilitate heat and mass transport, so that the lower input rate is requested to evaporate water for further increase in the feed velocity.

For PP membranes there is no significant variation in ΔT_f with the feed concentration (Fig. 5C), and so the influence of C_f on the energy input is less evident; the increase in C_f from 1.2 to 228 g L^{-1} at low feed velocity ($v_f < 4.8 \times 10^{-2}$ m s^{-1}) produces a slight increase in Q_{in}. At higher v_f ($>6.1 \times 10^{-2}$ m s^{-1}), Q_{in} decreases (slightly) monotonically with the salt concentration (Fig. 5B). These results, together with data of Table 3, demonstrate that for such kind of membranes the fluid-dynamic
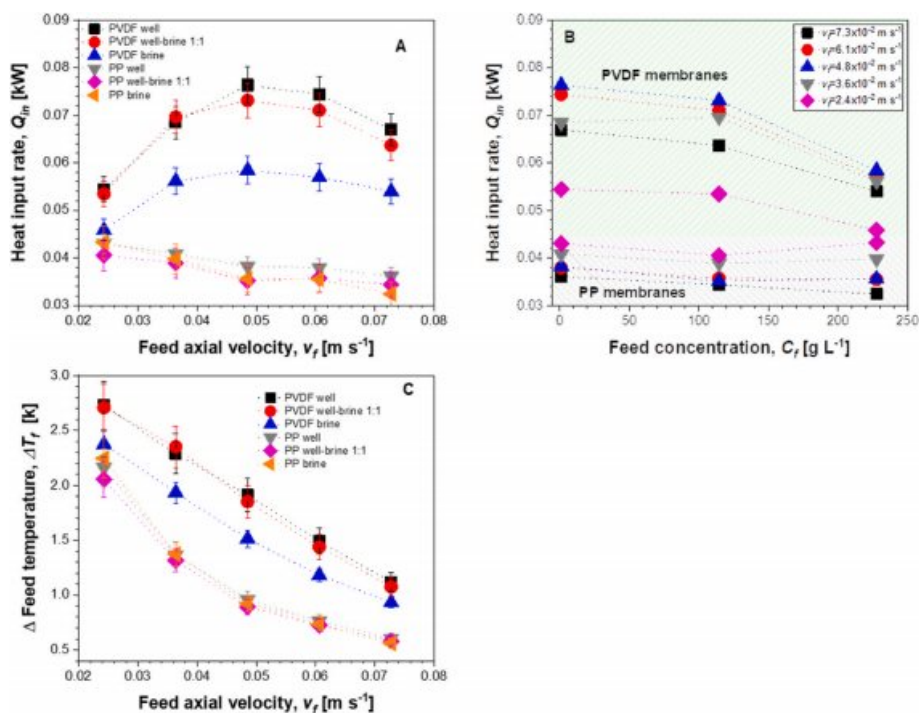

Fig. 5. Heat input rate Q_{in} as function of feed axial velocity v_f (A) and feed solution concentration C_f (B) for PP and PVDF membranes; (C) temperature variation ΔT_f between inlet and outlet stream on the feed side of the membrane module as function of solution velocity v_f for different solution compositions (well: 1.21 g L^{-1}; well-brine 1:1: 115 g L^{-1}; brine: 228 g L^{-1}) and membrane materials (dotted lines are guides for the eyes).

conditions of the feed are the most influencing parameters on the overall process performances in terms of heat (and mass) transfer coefficients. At low feed velocities, lower water fluxes are due to the presence of the relatively thick thermal boundary layer. As fluid velocity increases, enhanced heat and mass transport towards the boundary layers mitigates thermal (and concentration) polarizations and higher fluxes are obtained, despite the reduced fluid residence time within the membrane module. Therefore, assuming that heat and mass transport is the limiting step of the process, the reduced thermal conductivity of PP polymer (Table 2) allows the input heat to be more efficiently converted into latent heat of vaporization and be transported across the membrane by the evaporated water. This translates in the exponential-like decay of ΔT_f with the feed velocity of Fig. 5C and the continuous reduction in the requested energy input as feed velocity increases (in addition to the reduction of $C_{f,p}$ with C_f and despite the direct proportionality between Q_{in} and v_f in Eq. (7)), so that the monotonic decrease of Q_{in} with v_f is observed in Fig. 5A.

Based on the discussion above, it is clear the larger influence of heat transport through the membrane as limiting factor for PVDF membranes, while fluidynamic conditions affect mostly the performances of the PP membranes, which are seemingly more efficient to transport heat from the feed to the distillate side by the evaporated water. In addition, it is noteworthy the higher thermal energy input required for PVDF compared to PP membranes for the same operating conditions, despite the higher transmembrane fluxes of the latter over the entire range of investigated feed concentrations and velocities. This can be due to the effects of membranes physical properties, including the thermal conductivity k_m, on both permeate flux and thermal efficiency. Low k_m indicates a lower heat conductive membrane and hence high thermal (heat-transfer) resistance across the membrane matrix, which leads to less conductive heat loss [50]. The reduction of conductive heat loss results in a higher thermal efficiency which is the key variable in determining the lower Q_{in} values and improved permeation flux for PP samples. Furthermore, considering the conductivity of air/vapour being normally an order of magnitude lower than that of PP or PVDF polymers (k_g ranges between 0.02 and 0.03 W m^{-1} K^{-1} [33]), heat losses are minimized as the porosity and the thickness of the membrane increase.

Therefore, the lower thermal conductivity of the solid polymer and the higher porosity and thickness of PP membranes (Table 2) are responsible of the most efficient use of the input thermal energy to evaporate water. In addition, the higher porosity of the PP membranes contributes to higher mass transport due to the larger available area for the water vapour diffusion, so that high overall mass transfer coefficients are obtained for PP membranes (Fig. 3B) despite their larger thickness.

When dividing the heat input rates by the flow rates of water across the membrane (Eq. (6)), the specific thermal energy consumptions values showed in Fig. 6A and C are obtained. As expected, we found that the most energetically intensive conditions are associated to the use of PVDF membranes and when using feed solutions of increasing concentration. For both membrane type, the variation of the *STEC* with the feed velocity follows the behaviours of ΔT_f of Fig. 5C, with the splitting of the curves due to the different values of J_v for the diverse concentrations of the feed. The curves tend to merge when increasing feed velocity beyond 3.6×10^{-2} m s^{-1} due to the relatively steady flux at the high *Re* range, that provides a shift to the heat and mass transfer being controlled by the membrane rather than by the feed fluidynamics.

A common parameter useful to estimate the energy efficiency of an MD process is the gain to output ratio, which is defined as the ratio of heat associated with mass transfer to the energy input. The *GOR* reflects how well the energy input is utilized in the system for the production of water and the higher it is, the better is the performance of the system. *GOR* values calculated by Eq. (5) for the several tested conditions are reported in Fig. 6B and D. For PP membranes, the increase of *GOR* with v_f is more evident, due to the enhancement in water production and the reduction in heating duty that prevails on the increase of the feed flow rate. Therefore, for these membranes, the detrimental contribute to the *GOR* caused by the increase in feed velocity is overwhelmed by the increase in the transmembrane flux (Fig. 3A) and by the more efficient utilization of the input thermal energy (high J_v and low ΔT_f in Eq. (5)).

GOR data of Fig. 6 confirmed the energetic advantage of using PP membranes and the larger energy efficiency of the DCMD process for less-concentrated salt solutions, particularly at higher feed velocities. This is because the *GOR* decreases with increasing k_m regardless of the flow rate, due to the lower thermal resistance across the membrane and
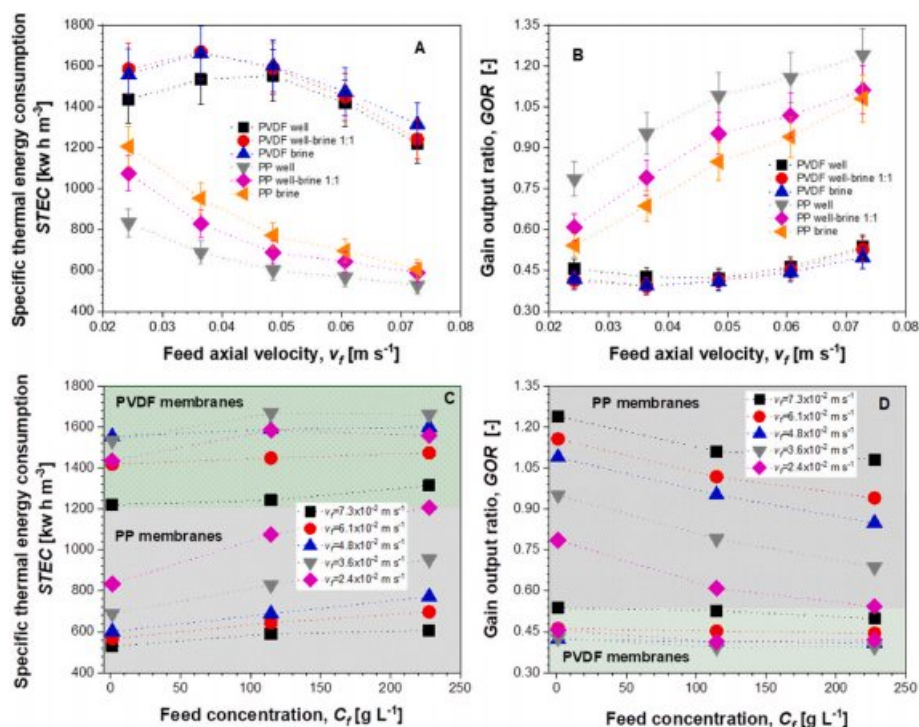

Fig. 6. Thermal energy calculations for the DCMD tests carried out at different feed axial velocities v_f, salt solution concentration C_f, and membrane type: (A) specific thermal energy consumption, *STEC*, and (B) gain to output ratio, *GOR*, as function of feed velocity, for different feed solution concentration (well: 1.21 g L^{-1}; well-brine 1:1: 115 g L^{-1}; brine: 228 g L^{-1}); (C) specific thermal energy consumption, *STEC*, and (D) gain to output ratio, *GOR*, as function of feed concentration C_f, for different feed velocities (dotted lines are guides for the eyes).

the greater conductive heat loss [51]. It was shown that variation in the thermal membrane conductivity from 0.05 to 0.45 W m^{-1} K^{-1} can reduce the thermal efficiency of MD from 80% to 40% [50]. The increased specific heat duty of PVDF membranes is then attributed to the consumption of a larger portion of the input thermal energy to compensate for the conductive heat loss which does not contribute to mass transfer.

Energy calculations demonstrated the higher values of *STEC* and lower values of *GOR* obtained for the DCMD system used in this work, compared to multi-effect MD or other MD configurations integrating energy recovery devices [52]. In the most favourable operative conditions, the energy penalty to be paid for DCMD in the logic of the integrated RED-MD system of Fig. 1, is comparable to the enthalpy of water vaporization (667 kWh m^{-3} for seawater at room temperature [40]). This energy duty is two to three orders of magnitude higher than the specific free energy of separation for seawater, which fixes the energy consumption in non-thermal desalination methods such as RO or ED (around to 2.58–8.5 kWh m^{-3} for seawater [52,53]). This makes the energy consumption in DCMD significant in comparison even with other thermal-based techniques like MSF and MED [45], demanding for further improvements to reduce *STEC* well below 100 kWh m^{-3}. However, the adoption of strategies finalized to capture and reuse the enthalpy of water vaporization by distillate condensation, either through multi-effect designs or by heat exchange between the influent feed stream and the exiting vapour distillate [54–57], or the use of low-grade (waste) thermal energy or renewable energy resources (such as solar [58,59]), is a key facet for the substantial reduction of energy consumption in MD applications.

4. Conclusions

Results of this study indicated that DCMD is a technically viable option to treat hypersaline outgoing solutions from a RED stage having a concentration which is practically impossible to be dewatered through RO, to produce pure water and high salinity stream to be recycled to the RED. Nevertheless, thermal energy calculations demonstrated the high values of *STEC* and low values of *GOR* obtained for the DCMD system used in this work, which is comparable to the enthalpy of water vaporization.

Most importantly, despite this high thermal energy duty, this work demonstrated the possibility to tailor the thermal energy requirements of the DCMD in the integrated RED-MD system, by modulating the volume ratio between the two streams that are partially mixed in the RED stage, together with the selection of the most suitable feed velocity. In addition, since DCMD can be driven by moderate feed temperatures, the use of low-grade (waste) heat or solar energy can increase the sustainability and the flexibility of the process, by adapting the water production rate to the available amount of thermal energy. When thermal energy is freely available (high insolation conditions or large amount of available low-grade heat), the shift towards the scenario 1 (high brine to well volume ratio at the RED stage) to dewater higher salinity stream in the MD unit will allow to harvest more SGP. In the conditions of reduced insolation (or limited amount of available low-grade heat), the system will move towards scenario 3, operating with more dilute streams (low brine to well volume ratios), thus reducing the thermal energy requirement while increasing the amount of water recovered.

In perspective, strategies aiming to capture and reuse the enthalpy of water vaporization by distillate condensation, together with improved control on the process with an artificial intelligence governing the switching of operation between the different scenarios depending on the available thermal energy, would represent a practicable solution for a substantial reduction of the energy request in MD processes while valorising the otherwise hazardous hypersaline brines.

Author contributions

G.D.P. & E.F. Conceptualization; E.P. & L.D. Data curation; L.D. Formal analysis; E.F. Funding acquisition; V.G. & E.P. Investigation; E.F. Methodology; G.D.P. Supervision; V.G. Validation; G.D.P. Visualization; G.D.P. & E.F. Writing - original draft; G.D.P., E.F., E.P., V.G. & L.D. Writing - review & editing.

Declaration of competing interest

The authors declare that they have no known competing financial interests or personal relationships that could have appeared to influence the work reported in this paper.

Data availability

Data will be made available on request.

Appendix A. Supplementary data

Supplementary data to this article can be found online at https://doi.org/10.1016/j.memsci.2023.121585.

References

[1] C.M. Anderson, R.S. DeFries, R. Litterman, P.A. Matson, D.C. Nepstad, S. Pacala, W.H. Schlesinger, M.R. Shaw, P. Smith, C. Weber, C.B. Field, Natural climate solutions are not enough, Science 363 (2019) 933–934, https://doi.org/10.1126/science.aaw2741.

[2] D. Welsby, J. Price, S. Pye, P. Ekins, Unextractable fossil fuels in a 1.5 °C world, Nature 597 (2021) 230–234, https://doi.org/10.1038/s41586-021-03821-8.

[3] F. Estrada, W.J.W. Botzen, Economic impacts and risks of climate change under failure and success of the Paris agreement, Ann. N. Y. Acad. Sci. 1504 (2021) 95–115, https://doi.org/10.1111/nyas.14652.

[4] A. Panagopoulos, K.-J. Haralambous, M. Loizidou, Desalination brine disposal methods and treatment technologies-A review, Sci. Total Environ. 693 (2019), 133545, https://doi.org/10.1016/j.scitotenv.2019.07.351.

[5] E. Jones, M. Qadir, M.T.H. van Vliet, V. Smakhtin, S. Kang, The state of desalination and brine production: a global outlook, Sci. Total Environ. 657 (2019) 1343–1356, https://doi.org/10.1016/j.scitotenv.2018.12.076.

[6] R. Einav, K. Harussi, D. Perry, The footprint of the desalination processes on the environment, Desalination 152 (2003) 141–154, https://doi.org/10.1016/S0011-9164(02)01057-3.

[7] A. Hashim, M. Hajjaj, Impact of desalination plants fluid effluents on the integrity of seawater, with the arabian gulf in perspective, Desalination 182 (2005) 373–393, https://doi.org/10.1016/j.desal.2005.04.020.

[8] D.A. Roberts, E.L. Johnston, N.A. Knott, Impacts of desalination plant discharges on the marine environment: a critical review of published studies, Water Res. 44 (2010) 5117–5128, https://doi.org/10.1016/j.watres.2010.04.036.

[9] O. Ogunbiyi, J. Saththasivam, D. Al-Masri, Y. Manawi, J. Lawler, X. Zhang, Z. Liu, Sustainable brine management from the perspectives of water, energy and mineral recovery: a comprehensive review, Desalination 513 (2021), 115055, https://doi.org/10.1016/j.desal.2021.115055.

[10] R. Pattle, Production of electric power by mixing fresh and salt water in the hydroelectric pile, Nature 174 (1954) 660, https://doi.org/10.1038/174660a0.

[11] Z. Wang, J. Li, C. Zhang, H. Wang, X. Kong, Power production from seawater and discharge brine of thermal desalination units by reverse electrodialysis, Appl. Energy 314 (2022), 118977, https://doi.org/10.1016/j.apenergy.2022.118977.

[12] C. Tristán, M. Fallanza, R. Ibáñez, I. Ortiz, Recovery of salinity gradient energy in desalination plants by reverse electrodialysis, Desalination 496 (2020), 114699, https://doi.org/10.1016/j.desal.2020.114699.

[13] E. Brauns, Towards a worldwide sustainable and simultaneous large-scale production of renewable and potable water through salinity gradient power by combining reversed electrodialysis and solar power? Desalination 219 (2008) 312–323, https://doi.org/10.1016/j.desal.2007.04.056.

[14] R.A. Tufa, S. Pawlowski, J. Veerman, K. Bouzek, E. Fontananova, G. Di Profio, S. Velizarov, J.G. Crespo, E. Nijmeijer, E. Curcio, Progress and prospects in reverse electrodialysis for salinity gradient energy conversion and storage, Appl. Energy 225 (2018) 290–331, https://doi.org/10.1016/j.apenergy.2018.04.111.

[15] A. Siria, P. Poncharal, A.-L. Biance, R. Fulcrand, X. Blase, S.T. Purcell, L. Bocquet, Giant osmotic energy conversion measured in a single transmembrane boron

nitride nanotube, Nature 494 (2013) 455–458, https://doi.org/10.1038/nature11876.

[16] J.W. Post, J. Veerman, H.V.M. Hamelers, G.J.W. Euverink, S.J. Metz, K. Nymeijer, C.J.N. Buisman, Salinity-gradient power: evaluation of pressure-retarded osmosis and reverse electrodialysis, J. Membr. Sci. 288 (2007) 218–230, https://doi.org/10.1016/j.memsci.2006.11.018.

[17] J.G. Hong, B. Zhang, S. Glabman, N. Uzal, X. Dou, H. Zhang, X. Wei, Y. Chen, Potential ion exchange membranes and system performance in reverse electrodialysis for power generation: a review, J. Membr. Sci. 486 (2015) 71–88, https://doi.org/10.1016/j.memsci.2015.02.039.

[18] IntelWATT project, case study 2: available at. https://www.intelwatt.eu/.

[19] M.S. Mauter, P.S. Fiske, Desalination for a circular water economy, Energy Environ. Sci. 13 (2020) 3180–3184, https://doi.org/10.1039/D0EE01653E.

[20] W. Wang, Y. Shi, C. Zhang, S. Hong, L. Shi, J. Chang, R. Li, Y. Jin, C. Ong, S. Zhuo, P. Wang, Simultaneous production of fresh water and electricity via multistage solar photovoltaic membrane distillation, Nat. Commun. 10 (2019) 3012, https://doi.org/10.1038/s41467-019-10817-6.

[21] T. Tong, M. Elimelech, The global rise of zero liquid discharge for wastewater management: drivers, technologies, and future directions, Environ. Sci. Technol. 50 (2016) 6846–6855, https://doi.org/10.1021/acs.est.6b01000.

[22] A.M. Alklaibi, N. Lior, Membrane-distillation desalination: status and potential, Desalination 171 (2005) 111–131, https://doi.org/10.1016/j.desal.2004.03.024.

[23] J. Kim, K. Park, D.R. Yang, S. Hong, A comprehensive review of energy consumption of seawater reverse osmosis desalination plants, Appl. Energy 254 (2019), 113652, https://doi.org/10.1016/j.apenergy.2019.113652.

[24] J. Sanmartino, M. Khayet, M. García-Payo, H. El-Bakouri, A. Riaza, Treatment of reverse osmosis brine by direct contact membrane distillation: chemical pretreatment approach, Desalination 420 (2017) 79–90, https://doi.org/10.1016/j.desal.2017.06.030.

[25] K.M. Shah, I.H. Billinge, X. Chen, H. Fan, Y. Huang, R.K. Winton, N. Yin Yip, Drivers, challenges, and emerging technologies for desalination of high-salinity brines: a critical review, Desalination 538 (2022), 115827, https://doi.org/10.1016/j.desal.2022.115827.

[26] M.P. Godino, L. Peña, C. Rincón, J.I. Mengual, Water production from brines by membrane distillation, Desalination 108 (1997) 91–97, https://doi.org/10.1016/S0011-9164(97)00013-1.

[27] L. Martínez-Díez, F.J. Florido-Díaz, Desalination of brines by membrane distillation, Desalination 137 (2001) 267–273, https://doi.org/10.1016/S0011-9164(01)00228-4.

[28] M.S. Osman, J.J. Schoeman, L.M. Baratta, Desalination/Concentration of reverse osmosis and electrodialysis brines with membrane distillation, Desalination Water Treat. 24 (2010) 293–301, https://doi.org/10.5004/dwt.2010.1657.

[29] R.A. Tufa, E. Curcio, E. Brauns, W. Baak, E. Fontananova, G. Di Profio, Membrane distillation and reverse electrodialysis for near-zero liquid discharge and low energy seawater desalination, J. Membr. Sci. 496 (2015) 325–333, https://doi.org/10.1016/j.memsci.2015.09.008.

[30] R.A. Tufa, Y. Noviello, G. Di Profio, F. Macedonio, A. Ali, E. Drioli, E. Fontananova, K. Bouzek, E. Curcio, Integrated membrane distillation-reverse electrodialysis system for energy-efficient seawater desalination, Appl. Energy 253 (2019), 113551, https://doi.org/10.1016/j.apenergy.2019.113551.

[31] J.D. Gil, L. Roca, G. Zaragoza, M. Pérez, M. Berenguel, Improving the performance of solar membrane distillation processes for treating high salinity feeds: a process control approach for cleaner production, J. Clean. Prod. 338 (2022), 130446, https://doi.org/10.1016/j.jclepro.2022.130446.

[32] https://cordis.europa.eu/project/id/958454/results.

[33] J. Phattaranawik, R. Jiraratananon, A.G. Fane, Heat transport and membrane distillation coefficients in direct contact membrane distillation, J. Membr. Sci. 212 (2003) 177–193, https://doi.org/10.1016/S0376-7388(02)00498-2.

[34] A. Khalifa, H. Ahmad, M. Antar, T. Laoui, M. Khayet, Experimental and theoretical investigations on water desalination using direct contact membrane distillation, Desalination 404 (2017) 22–34, https://doi.org/10.1016/j.desal.2016.10.009.

[35] L. Matìnez-Dìez, M.I. Vàzquez-Gonzàlez, Temperature and concentration polarization in membrane distillation of aqueous salt solutions, J. Membr. Sci. 156 (1999) 265–273, https://doi.org/10.1016/S0376-7388(98)00349-4.

[36] S. Bouguecha, R. Chouikh, M. Dhahbi, Numerical study of the coupled heat and mass transfer in membrane distillation, Desalination 152 (2002) 245–252, https://doi.org/10.1016/S0011-9164(02)01070-6.

[37] J.M. Rodriquez-Maroto, L. Martinez-Diez, Bulk and measured temperatures in direct contact membrane distillation, J. Membr. Sci. 250 (2005) 141–149, https://doi.org/10.1016/j.memsci.2004.09.046.

[38] G. Zuo, R. Wang, R. Field, A.G. Fane, Energy efficiency evaluation and economic analyses of direct contact membrane distillation system using Aspen Plus, Desalination 283 (2011) 237–244, https://doi.org/10.1016/j.desal.2011.04.048.

[39] K.W. Lawson, D.R. Lloyd, Membrane distillation, J. Membr. Sci. 124 (1997) 1–25, https://doi.org/10.1016/S0376-7388(96)00236-0.

[40] M.H. Sharqawy, J.H. Lienhard V, S.M. Zubair, Thermophysical properties of seawater: a review of existing correlations and data, Desalination Water Treat. 16 (2010) 354–380, https://doi.org/10.5004/dwt.2010.1079.

[41] G.R. Carvalho, F. Chenlo, R. Moreira, J. Telis-Romero, Physicothermal properties of aqueous sodium chloride solutions, J. Food Process. Eng. 38 (2015) 234–242, https://doi.org/10.1111/jfpe.12160.

[42] P. Olynyk, A.R. Gordon, The vapor pressure of aqueous solutions of sodium chloride at 20, 25 and 30° for concentrations from 2 molal to saturation, J. Am. Chem. Soc. 65 (1943) 224–226, https://doi.org/10.1021/ja01242a023.

[43] M.-C. Sparenberg, B. Hanot, C. Molina-Fernández, P. Luis, Experimental mass transfer comparison between vacuum and direct contact membrane distillation for the concentration of carbonate solutions, Separ. Purif. Technol. 275 (2021), 119193, https://doi.org/10.1016/j.seppur.2021.119193.

[44] A. Al-Karaghouli, L.L. Kazmerski, Energy consumption and water production cost of conventional and renewable-energy-powered desalination processes, Renew. Sustain. Energy Rev. 24 (2013) 343–356, https://doi.org/10.1016/j.rser.2012.12.064.

[45] A. Deshmukh, C. Boo, V. Karanikola, S. Lin, A.P. Straub, T. Tong, D.M. Warsinger, M. Elimelech, Membrane distillation at the water-energy nexus: limits, opportunities, and challenges, Energy Environ. Sci. 11 (2018) 1177–1196, https://doi.org/10.1039/C8EE00291F.

[46] D. Brogioli, F. La Mantia, N.Y. Yip, Thermodynamic analysis and energy efficiency of thermal desalination processes, Desalination 428 (2018) 29–39, https://doi.org/10.1016/j.desal.2017.11.010.

[47] M.H. Sharqawy, J.H. Lienhard, S.M. Zubair, Thermophysical properties of seawater: a review of existing correlations and data, Desalination Water Treat. 16 (2012) 354–380, https://doi.org/10.5004/dwt.2010.1079.

[48] Engineering ToolBox, Water - heat of vaporization vs. Temperature, Available at: https://www.engineeringtoolbox.com/water-properties-d_1573.html, 2010.

[49] M.L.V. Ramires, C.A. Nieto de Castro, J.M.N.A. Fareleira, W.A. Wakeham, Thermal conductivity of aqueous sodium chloride solutions, J. Chem. Eng. Data 39 (1994) 186–190, https://doi.org/10.1021/je00013a053.

[50] S. Al-Obaidani, E. Curcio, F. Macedonio, G. Di Profio, H. Al-Hinai, E. Drioli, Potential of membrane distillation in seawater desalination: thermal efficiency, sensitivity study and cost estimation, J. Membr. Sci. 323 (2008) 85–98, https://doi.org/10.1016/j.memsci.2008.06.006.

[51] A.M. Alklaibi, N. Lior, Heat and mass transfer resistance analysis of membrane distillation, J. Membr. Sci. 282 (2006) 362–369, https://doi.org/10.1016/j.memsci.2006.05.040.

[52] M. Elimelech, W.A.W. Phillip, The future of seawater desalination: energy, technology, and the environment, Science (New York, N.Y.) (2011) 712–717, https://doi.org/10.1126/science.1200488.

[53] H. Nassrullah, S.F. Anis, R. Hashaikeh, N. Hilal, Energy for desalination: a state-of-the-art review, Desalination 491 (2020), 114569, https://doi.org/10.1016/j.desal.2020.114569.

[54] J.A. Andrés-Mañas, A. Ruiz-Aguirre, F.G. Acién, G. Zaragoza, Performance increase of membrane distillation pilot scale modules operating in vacuum enhanced air-gap configuration, Desalination 475 (2020), https://doi.org/10.1016/j.desal.2019.114202.

[55] E.K. Summers, H.A. Arafat, J.H. Lienhard, Energy efficiency comparison of single stage membrane distillation (MD) desalination cycles in different configurations, Desalination 290 (2012) 54–66, https://doi.org/10.1016/j.desal.2012.01.004.

[56] K. Zhao, W. Heinzl, M. Wenzel, S. Büttner, F. Bollen, G. Lange, S. Heinzl, N. Sarda, Experimental study of the memsys vacuum-multi-effect-membrane-distillation (VMEMD) module, Desalination 323 (2013) 150–160, https://doi.org/10.1016/j.desal.2012.12.003.

[57] J.A. Andrés-Mañas, I. Requena, G. Zaragoza, Characterization of the use of vacuum enhancement in commercial pilot-scale air gap membrane distillation modules with different designs, Desalination 528 (2022), 115490, https://doi.org/10.1016/j.desal.2021.115490.

[58] P.D. Dongare, A. Alabastri, S. Pedersen, K.R. Zodrow, N.J. Hogan, O. Neumann, J. Wu, T. Wang, A. Deshmukh, M. Elimelech, Q. Li, P. Nordlander, N.J. Halas, Nanophotonics-enabled solar membrane distillation for off-grid water purification, Proc. Natl. Acad. Sci. U.S.A. 114 (2017) 6936–6941, https://doi.org/10.1073/pnas.1701835114.

[59] J.A. Andrés-Mañas, L. Roca, A. Ruiz-Aguirre, F.G. Acién, J.D. Gil, G. Zaragoza, Application of solar energy to seawater desalination in a pilot system based on vacuum multi-effect membrane distillation, Appl. Energy 258 (2020), 114068, https://doi.org/10.1016/j.apenergy.2019.114068.